Chapter 12
Verification and Convergence of Multi-Harmonic Balance Algorithms for Future Application in Sierra/SD Finite Element Code

Oliver Khan, Dalton L. Stein, Nathan Schill, Robert J. Kuether, and David M. Day

Keywords Harmonic balance · Numerical continuation · Forced response curves · Nonlinear vibrations

Background

Engineered structures are frequently subjected to cyclic loading. Examples include rotating compressor blades in aircraft engines [1], buildings subjected to alternating heating and cooling cycles [2], and materials that are periodically stretched and compressed during testing [3]. Since cyclic loading is so prevalent, engineering industries have sought tools for predicting a structure's steady-state response to time-periodic forcing, particularly in the presence of nonlinearities. A common approach is to discretize a structure into a finite element model and use numerical time integration (TI) to compute the response over time. Although TI captures stable periodic orbits with high accuracy, small time-steps are needed to resolve high-frequency oscillations and long integration times are often required for the response to converge to a steady state. As an alternative to TI, the method of multi-harmonic balance (MHB) is increasingly adopted in mechanics and dynamics research to approximate the steady-state response of a nonlinear system to a time-periodic input. MHB represents the response as a finite Fourier series in time, and then applies a Fourier–Galerkin projection to the spatially-discretized governing equations from a finite element model. This yields a set of nonlinear algebraic equations for the Fourier coefficients of the response, which are solved using iterative techniques such as the Newton–Raphson method [4]. This approach offers efficiency by directly solving for the steady-state response, unlike TI which must process transient dynamics before reaching the steady state. When combined with numerical continuation [5], MHB can also compute a curve of periodic solutions as a parameter is varied. A notable example is the forced response curve (FRC), which shows the amplitude of a steady-state response as a (possibly multivalued) function of the forcing frequency. While TI only captures stable periodic orbits, MHB computes both stable and unstable solutions along an FRC, providing a more complete picture of a system's dynamics [4].

Despite its promise, the computational cost of MHB can increase significantly with the number of Fourier harmonics used, particularly for large-scale models. This occurs because the number of algebraic equations to be solved scales as $(2N_h + 1)n$, where N_h is the number of Fourier harmonics and n is the number of degrees of freedom in the finite element

Oliver Khan
Stanford University, Department of Mechanical Engineering
e-mail: ogkhan@stanford.edu

Dalton L. Stein
University of Rhode Island, Department of Mechanical, Industrial and Systems Engineering
e-mail: daltonstein98@uri.edu

Nathan Schill
Brigham Young University, Department of Mathematics
e-mail: schilln@mathematics.byu.edu

Robert J. Kuether · David M. Day
Sandia National Laboratories*
e-mail: rjkueth@sandia.gov; dmday@sandia.gov

*Sandia National Laboratories is a multimission laboratory managed and operated by National Technology and Engineering Solutions of Sandia, LLC., a wholly owned subsidiary of Honeywell International, Inc., for the U.S. Department of Energy's National Nuclear Security Administration under contract DE-NA-0003525.

© The Author(s), under exclusive license to River Publishers 2026

Kristin B. Zimmerman, PhD (eds.), *Topics in Modal Analysis & Parameter Identification in Structural Dynamics, 2026, Vol. 8*,
Conference Proceedings of the Society for Experimental Mechanics Series, https://doi.org/10.13052/rp-9788743814191

model. Understanding the convergence properties of MHB and determining the necessary Fourier basis for accurate solutions are crucial. While MHB is popular in research, its integration into commercial software remains limited, though some advancements have been made in MSC Nastran [6] and ANSYS [7]. The objective of the present work was to expand the utility of MHB in large-scale commercial codes by preparing an MHB algorithm for implementation in Sierra/Structural Dynamics (SD) finite element code at Sandia National Laboratories. Building upon an existing MATLAB implementation of MHB with pseudo-arclength continuation [4], an improved MHB algorithm was written in Sierra/SD's native language, C++. This C++ implementation and the original MATLAB implementation were verified by comparing FRCs with those computed using TI. It was important to verify both codes because the C++ algorithm was intended for future use in Sierra/SD and the MATLAB algorithm formed the basis of the C++ algorithm. After verification, the convergence of the C++ and MATLAB MHB algorithms was assessed for varying numbers of harmonics. The error metrics used in the convergence study were then used to create an adaptive algorithm that automatically selected the harmonics included in the response. In the future, this work will lay the groundwork for further MHB developments in Sandia's finite element codes, aimed at addressing challenges such as frictional damping and nonlinear viscoelastic behavior.

Implementation of Multi-Harmonic Balance

The multi-harmonic balance (MHB) algorithms in C++ and MATLAB required knowledge of spatially-discretized governing equations of the form

$$\mathbf{M}\ddot{\mathbf{x}} + \mathbf{C}\dot{\mathbf{x}} + \mathbf{K}\mathbf{x} + \mathbf{f}_{\text{nl}}(\mathbf{x}, \dot{\mathbf{x}}) = \mathbf{f}_{\text{pre}} + \mathbf{f}_{\text{ext}}(t), \tag{1}$$

where $\mathbf{M}, \mathbf{C}$, and $\mathbf{K}$ were the linear mass, damping, and stiffness matrices, respectively; $\mathbf{f}_{\text{nl}}(\mathbf{x}, \dot{\mathbf{x}})$ was the vector of nonlinear internal forces; $\mathbf{f}_{\text{pre}}$ was the constant preload force; and $\mathbf{f}_{\text{ext}}(t)$ was the time-periodic external force with fundamental frequency ω. The displacement vector $\mathbf{x}(t) \in \mathbb{R}^n$ was approximated by the truncated Fourier series,

$$\mathbf{x}(t) = \frac{\mathbf{c}_0^x}{\sqrt{2}} + \sum_{k=1}^{N_h} [\mathbf{c}_k^x \cos(k\omega t) + \mathbf{s}_k^x \sin(k\omega t)], \tag{2}$$

which converged based on the number of harmonics, N_h, included in the expansion. Substituting Eq. (2) into Eq. (1) and performing a Fourier-Galerkin projection onto the first N_h harmonics yielded a system of nonlinear algebraic equations for the Fourier coefficients $\mathbf{z} = \begin{bmatrix}(\mathbf{c}_0^x)^\top & (\mathbf{c}_1^x)^\top & (\mathbf{s}_1^x)^\top & \cdots & (\mathbf{c}_{N_h}^x)^\top & (\mathbf{s}_{N_h}^x)^\top\end{bmatrix}^\top$ of the displacement $\mathbf{x}$:

$$\mathbf{r}(\mathbf{z}, \omega) = \mathbf{A}(\omega)\mathbf{z} + \mathbf{b}_{\text{nl}}(\mathbf{z}) - \mathbf{b}_{\text{pre}} - \mathbf{b}_{\text{ext}} = \mathbf{0}. \tag{3}$$

In Eq. (3), $\mathbf{A}(\omega)$ encompassed the linear dynamics obtained from Fourier-Galerkin projection; $\mathbf{b}_{\text{nl}}$, $\mathbf{b}_{\text{pre}}$, and $\mathbf{b}_{\text{ext}}$ were Fourier coefficients of the nonlinear, preload, and time-periodic external forces, respectively; and $\mathbf{r}(\mathbf{z}, \omega) \in \mathbb{R}^m$ was the frequency domain residual with $m = (2N_h + 1)n$ being the problem dimension. In the numerical continuation procedure, ω was unknown at each step beyond the initial starting frequency. In order to solve for both $\mathbf{z}$ and ω at subsequent locations along an FRC, an additional constraint equation was appended to Eq. (3) such that the residual function became

$$\tilde{\mathbf{r}}(\mathbf{y}) = \begin{bmatrix} \mathbf{A}(\omega)\mathbf{z} + \mathbf{b}_{\text{nl}}(\mathbf{z}) - \mathbf{b}_{\text{pre}} - \mathbf{b}_{\text{ext}} \\ \mathbf{V}^\top(\mathbf{y} - \mathbf{y}^{(k=1)}) \end{bmatrix} = \mathbf{0}, \tag{4}$$

where $\mathbf{y} = \begin{bmatrix}\mathbf{z}^\top & \omega\end{bmatrix}^\top \in \mathbb{R}^{m+1}$ was the augmented vector of unknowns. Equation (4) was solved using Newton-Raphson iterations to a specified tolerance, ε_h.

Distinct Features of C++ Multi-Harmonic Balance Algorithm

The existing MATLAB MHB implementation utilized direct solves of the linear systems arising in the predictor-corrector scheme, which was known to be a substantial bottleneck in MHB continuation [4]. This work aimed to extend the work done in [4] and develop a code specifically tailored to large-scale systems. Therefore, the new C++ implementation utilized Krylov subspace methods to iteratively solve the linear systems during each continuation step. A known challenge for iterative methods in path-following problems was that the constraint equation could only be approximately satisfied due to the tolerance set for the iterative solver. To overcome this, the non-augmented Jacobian derived from Eq. (3) was mapped through a linear transformation matrix, $\mathbf{Q} \in \mathbb{R}^{m+1 \times m}$, such that the constraint equation was enforced on the iterates of the Krylov method. The construction of $\mathbf{Q}$ was based on Householder transformations, as outlined in [8]. The iterative solver used here was the bi-conjugate gradient stabilized method (BiCGSTAB) [9].

Verification

The C++ and MATLAB MHB implementations were verified on two related benchmark systems shown in Fig. 1. The cantilever beam in Fig. 1a was meshed with 10 Euler–Bernoulli beam elements, yielding 10 rotational and 10 translational degrees of freedom. Table 1 contains further details on the spatial geometry and material properties of the beam, as well as the cubic nonlinear spring attached to the beam's free end.

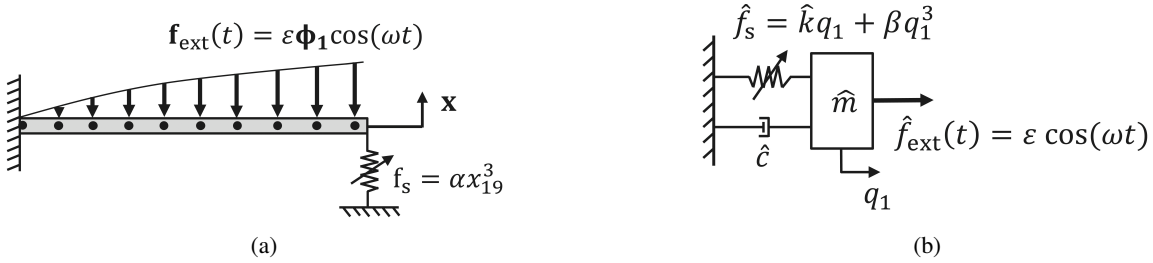

Fig. 1 (a) Model of the cantilever beam with cubic spring and (b) the Duffing oscillator obtained by projecting the beam-spring model onto its first linear normal mode.

Table 1 Parameters for Cantilever Beam Finite Element Model

Length × Width × Thickness [m]	$1 \times 0.00635 \times 0.003175$
Young's Modulus [GPa]	70
Density [kg m^{-3}]	2880
Modal Damping Ratio, ζ [%]	0.75
Nonlinear Spring Stiffness, α [N m^{-3}]	518.7

The Duffing oscillator in Fig. 1b was a single-degree-of-freedom reduced-order model of the beam-spring system obtained by projecting the full-order model onto its first linear normal mode, ϕ_1. The Duffing oscillator's governing equation was given by

$$\ddot{q}_1 + 2\zeta\omega_1\dot{q}_1 + \omega_1^2 q_1 + \beta q_1^3 = \varepsilon\cos(\omega t), \tag{5}$$

where q_1 was the modal displacement of ϕ_1, $\zeta = 0.0075$, $\omega_1 = 15.9$ rad s^{-1}, $\beta = 10^6$, and $\varepsilon = 0.025$.

Convergence

Three approaches were taken to assess the convergence of the C++ and MATLAB MHB codes: (i) a residual equation defined in the time domain, (ii) a residual equation defined in the frequency domain, and (iii) the magnitudes of individual harmonics in the computed displacement $\mathbf{x}$. The time-domain and frequency-domain residuals were defined by Eq. (6) and Eq. (7), respectively, and measured how well $\mathbf{x}$ and $\mathbf{z}$ satisfied the system dynamics:

$$\mathbf{R}(t) = \mathbf{M}\ddot{\mathbf{x}} + \mathbf{C}\dot{\mathbf{x}} + \mathbf{K}\mathbf{x} + \mathbf{f}_{\text{nl}}(\mathbf{x}, \dot{\mathbf{x}}) - \mathbf{f}_{\text{pre}} - \mathbf{f}_{\text{ext}}(t) \tag{6}$$

$$\mathbf{r}_{N_h^r}(\mathbf{z}, \omega) = \mathbf{A}(\omega)\mathbf{z} + \mathbf{b}_{\text{nl},N_h^r}(\mathbf{z}) - \mathbf{b}_{\text{pre}} - \mathbf{b}_{\text{ext}}. \tag{7}$$

Equation (7) is re-written distinct from Eq. (3) to emphasize the role of N_h^r, the number of harmonics assumed in the discrete Fourier transform when computing the Fourier coefficients of the nonlinear forcing, $\mathbf{b}_{\text{nl}}$, using the alternating frequency/time method [1, 4]. When first computing the solution $\mathbf{z}$ during the numerical continuation procedure, N_h^r was set equal to N_h, meaning that the number of harmonics in the nonlinear force vector, $\mathbf{b}_{\text{nl}}$, was the same as the number of harmonics included in the response, $\mathbf{z}$. However, when assessing the convergence of the MHB algorithms, N_h^r was set larger than N_h to study the change in the frequency domain residual, $\mathbf{r}_{N_h^r}$, when additional harmonics were accounted for in the nonlinear force vector but not in the response. This provided a relative metric to assess the increase or decrease in accuracy of a solution $\mathbf{z}$ that accounted for more or fewer of the higher harmonics introduced by the nonlinear forcing. After solving

for $\mathbf{R}$ and $\mathbf{r}_{N_h^r}$ in Eqs. (6)–(7), dimensionless error metrics were defined by normalizing the magnitudes of the time and frequency domain residuals by the magnitudes of the external forces:

$$E_{\mathbf{x}} = \frac{\|\mathbf{R}\|_{L^2([0,\,2\pi/\omega])}}{\|\mathbf{f}_{\text{pre}} + \mathbf{f}_{\text{ext}}\|_{L^2([0,\,2\pi/\omega])}} \tag{8}$$

$$E_{\mathbf{z}} = \frac{\|\mathbf{r}_{N_h^r}\|_2}{\|\mathbf{b}_{\text{pre}} + \mathbf{b}_{\text{ext}}\|_2}. \tag{9}$$

For a given fundamental forcing frequency ω, the L^2 norm of the time domain residual $\mathbf{R}(t)$ (and analogously, the external forces) over a single oscillation period was:

$$\|\mathbf{R}\|_{L^2([0,\,2\pi/\omega])} = \sqrt{\int_0^{2\pi/\omega} \mathbf{R}^\top(t)\mathbf{R}(t)\,dt}. \tag{10}$$

Separate from the error metrics $E_{\mathbf{x}}$ and $E_{\mathbf{z}}$ defined above, the magnitudes of the coefficients of the solution $\mathbf{z}$ were examined for different values of ω. Following [10], the coefficient magnitudes were normalized by the norm of the solution $\mathbf{z}$, such that $|\hat{\mathbf{z}}_i|/\|\mathbf{z}\| := \sqrt{\|\mathbf{c}_i^x\|^2 + \|\mathbf{s}_i^x\|^2}/\|\mathbf{z}\|$ represented the fraction of the solution's spectral energy contained in the i-th harmonic. Together, the error metrics given by Eq. (8) and Eq. (9), along with the spectral energy contained in the i-th harmonic, were used to explore an adaptive harmonic selection algorithm, which will be discussed in the presentation.

Results

For brevity, verification and convergence results are only shown for the cantilever beam. Analogous results for the Duffing oscillator will be provided in the presentation. Figure 2a shows forced response curves (FRCs) computed with time integration (TI), as well as the C++ and MATLAB multi-harmonic balance (MHB) algorithms with five harmonics included in the response (denoted H_5). All three methods showed strong agreement with each other, providing evidence that the C++ and MATLAB algorithms were implemented correctly. Figure 2b, meanwhile, shows the normalized L^2 norm of the time domain residual as a function of forcing frequency for odd numbers of harmonics. (Even harmonic orders are not shown because the cubic nonlinearity of the spring caused odd harmonics to dominate the response.) As the number of harmonics

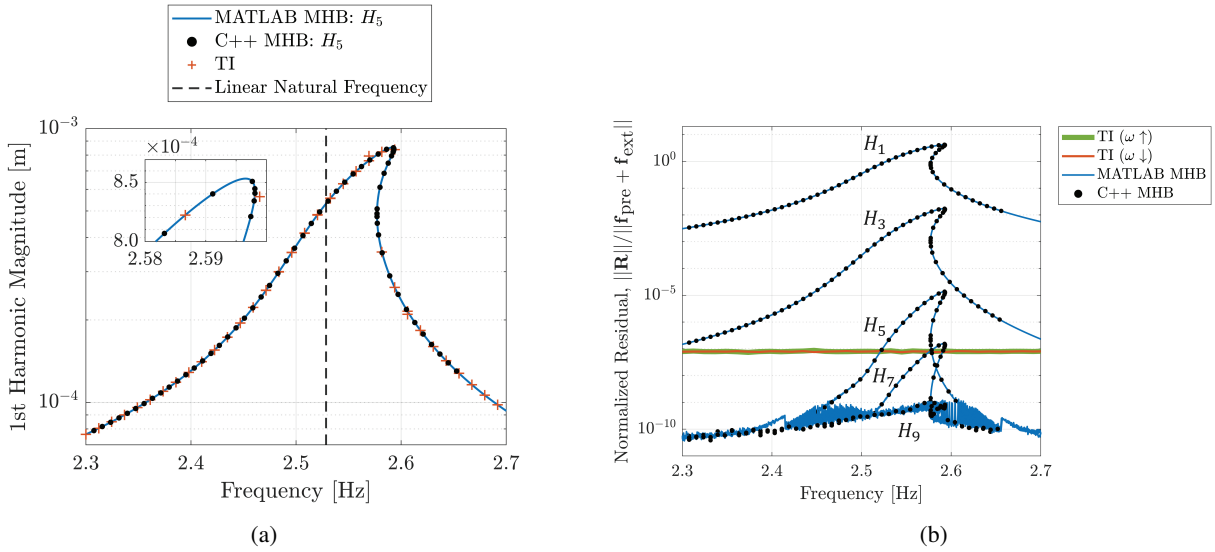

(a) (b)

Fig. 2 (a) First harmonic of the beam tip displacement, x_{19}, vs. forcing frequency and (b) normalized L^2 norm of the time domain residual vs. forcing frequency, for time integration (TI) and multi-harmonic balance (MHB) implementations in C++ and MATLAB. The notation H_j means that $N_h = j$ harmonics were included in the Fourier series expansion of the response in MHB. Note that in (a), the plus markers represent TI for both increasing and decreasing ω, while in (b), the TI data is separated based on whether ω was increasing ($\uparrow$) or decreasing ($\downarrow$).

included in MHB increased from one (H_1) to nine (H_9), the residual magnitude decreased, indicating that the approximation to the response became more accurate with more harmonics. The largest residual magnitudes coincided with the peak of the FRC. This higher error near the peak helped explain the small discrepancy between TI and the MHB algorithms in Fig. 2a near a forcing frequency of 2.595 Hz (see inset). Furthermore, the C++ and MATLAB MHB algorithms had nearly identical residual magnitudes in Fig. 2b for all harmonic orders. This agreement between the C++ and MATLAB residuals served as another form of verification, as it suggested that both algorithms were computing the same solutions at each harmonic order. It was also important to observe that the C++ and MATLAB normalized residual magnitudes in Fig. 2b saturated near 10^{-10}. This represented the limit of maximum possible accuracy given the C++ algorithm's linear solve tolerance and the MATLAB algorithm's residual tolerance. Increasing the harmonic order beyond nine had diminishing returns on accuracy unless the tolerances of the MHB solvers were lowered.

Acknowledgments This research was conducted at the 2025 Nonlinear Mechanics and Dynamics Research Institute hosted by Sandia National Laboratories and the University of New Mexico. Sandia National Laboratories is a multimission laboratory managed and operated by National Technology and Engineering Solutions of Sandia, LLC., a wholly owned subsidiary of Honeywell International, Inc., for the U.S. Department of Energy's National Nuclear Security Administration under contract DE-NA-0003525.

References

1. Y. Colaïtis and A. Batailly, "The harmonic balance method with arc-length continuation in blade-tip/casing contact problems," Journal of Sound and Vibration, vol. 502, p. 116070, 2021.
2. A. Athienitis, "A methodology for integrated building–HVAC system thermal analysis," Building and Environment, vol. 28, no. 4, pp. 483–496, 1993.
3. S. Patra, P. M. Ajayan, and T. N. Narayanan, "Dynamic mechanical analysis in materials science: The Novice's Tale," Oxford Open Materials Science, vol. 1, p. itaa001, Jan. 2021.
4. R. Kuether and A. Steyer, "Large-scale harmonic balance simulations with Krylov subspace and preconditioner recycling," Nonlinear Dynamics, vol. 112, pp. 1–22, 2024.
5. R. Seydel, *Practical Bifurcation and Stability Analysis*, vol. 5, Springer Science & Business Media, 2009.
6. D. Najera-Flores and R. J. Kuether, "Application of multi-harmonic balance for nonlinear frequency response analysis in MSC Nastran," presented at the 40th International Modal Analysis Conference (IMAC XL), 2022.
7. M. Kwarta, "An overview of ANSYS harmonic balance method: Current capabilities and future directions," presented at the 43rd International Modal Analysis Conference (IMAC XLIII), 2025.
8. H. F. Walker, "An Adaptation of Krylov Subspace Methods to Path Following Problems," SIAM Journal on Scientific Computing, vol. 21, no. 3, pp. 1191–1198, 1999.
9. H. A. van der Vorst, "Bi-CGSTAB: A fast and smoothly converging variant of Bi-CG for the solution of nonsymmetric linear systems," SIAM Journal on Scientific and Statistical Computing, vol. 13, no. 2, pp. 631–644, 1992.
10. A. Grolet and F. Thouverez, "On a new harmonic selection technique for harmonic balance method," Mechanical Systems and Signal Processing, vol. 30, pp. 43–60, 2012.